Single-stage vibratory gyroscope control methods for direct angle measurements

2011 Meas. Sci. Technol. 22 055201

(http://iopscience.iop.org/0957-0233/22/5/055201)

Meas. Sci. Technol. **22** (2011) 055201 (11pp) doi:10.1088/0957-0233/22/5/055201

Single-stage vibratory gyroscope control methods for direct angle measurements

Chien-Yu Chi and Tsung-Lin Chen

Department of Mechanical Engineering, National Chiao Tung University, Hsinchu, Taiwan 30056, Republic of China

E-mail: tsunglin@mail.nctu.edu.tw

Received 10 August 2010, in final form 18 February 2011
Published 13 April 2011
Online at stacks.iop.org/MST/22/055201

Abstract

This paper presents a control algorithm that can compensate for imperfect dynamics of vibrating gyroscopes. The compensated gyroscope dynamics can directly measure the rotation angle without integrating the angular rate. The direct angle measurement approach is promising because it is exempt from the error accumulation problem. However, using control methods to compensate for imperfect dynamics for the direct angle measurement is very challenging work, and very few control algorithms were reported to achieve that. Different from existing approaches, the proposed method has the following advantages: it requires the measurements of either the proof mass velocity or position, it does not require a calibration phase prior to normal use, and it compensates different types of imperfection even when the proof mass of a gyroscope is unknown. In a demonstration case, imperfections cause system parameters 20% deviated from their designated values; the measured signals are the proof mass velocities and contaminated by zero-mean white noise with a noise level of 0.1% full scale output (FSO); the angular rate to be measured is $200\sin(2\pi \times 10t)\,\mathrm{deg\,s^{-1}}$. The proposed algorithm can compensate for those imperfections and achieve an angle measurement accuracy of 0.23°.

Keywords: MEMS vibratory gyroscopes, direct angle measurement, state observer

(Some figures in this article are in colour only in the electronic version)

1. Introduction

MEMS gyroscopes are typically designed to be angular rate sensors, and ideally, the rotation angle can be obtained by integrating the angular rates. In practice, the bias and noise existed in the measured angular rates cause the estimated angles to drift over time [1]. This error accumulation problem can be comprehended by an example shown in figure 1. The upper plot shows a random signal with zero mean. Integrating this signal over time produces a 'random walk' signal shown as one line in the middle plot. If this integration process is carried out several times (in this case, ten zero-mean random signals which lead to ten random walk signals), one can show that the standard deviation of the random walk signal increases with time.

In 1978, Friedland and Hutton suggested the use of a vibratory gyroscope for measuring rotation angles [2]. Their research showed that the precession angle of the proof mass trajectory, induced by the Coriolis force only, equals the rotation angle to be measured (see figure 2). This precession angle can be calculated by the instantaneous values of the proof mass position and velocity. Thus, there is no error accumulation problem in obtaining the rotation angle. Specifically, to achieve the precession induced by the Coriolis force only, the vibratory gyroscope must consistently oscillate along two axes at the same resonant frequency, no cross-axis dynamics coupling except the coupling induced by the Coriolis force.

A MEMS vibratory gyroscope can hardly have the dynamics discussed above because the MEMS fabrication process and structure designs can easily cause mechanical structure imperfections. Those imperfections mainly come from the dimension variations, residual film stress, layer misalignment, etc [3, 4]. All these errors cause the fabricated gyroscope parameters (mass, spring constants, damping coefficients) to deviate from their designated values.

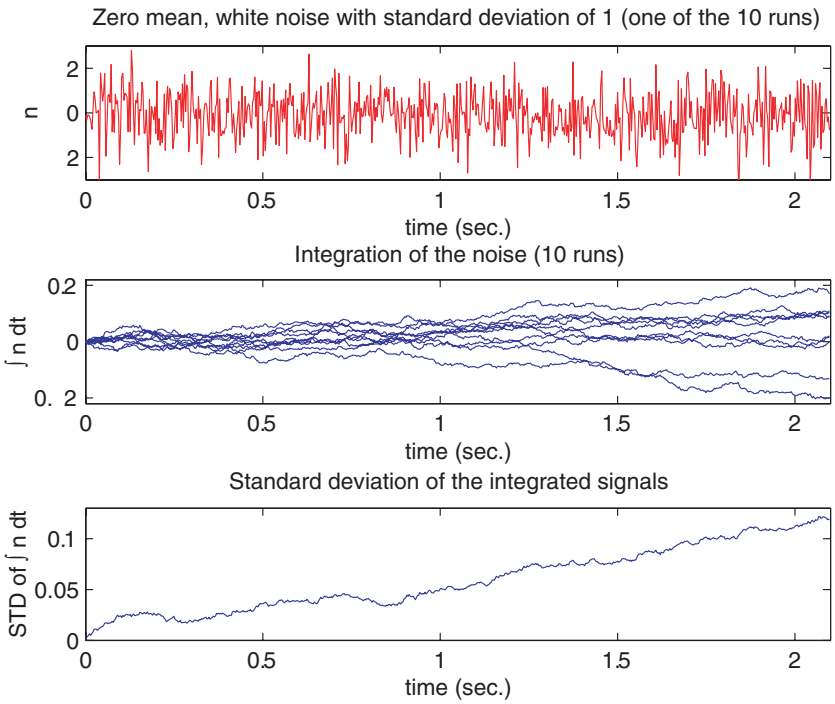

Figure 1. Signal drifts due to integrating zero-mean white noises. Ten random signals are generated and integrated over time. The top plot shows one of the ten signals; the middle plot shows the ten signals after integration; the bottom plot shows the standard deviation of the integrated signals.

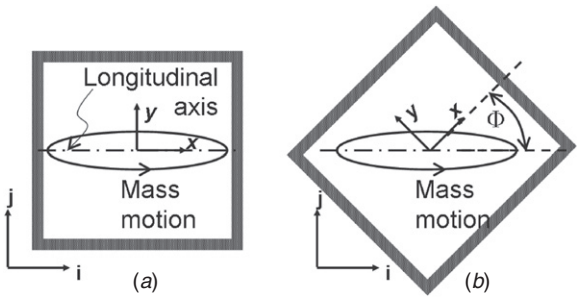

Figure 2. Illustration of precession caused by Coriolis force. (i, j) is an inertial frame, (x, y) is the rotation frame, and ϕ is the precession angle. (a) An initial state, (b) after the gyroscope rotates 45°.

Even worse, they induce cross-axis resilient force and cross-axis damping force, which lead to the serious 'quadrature error' in gyroscope systems [3]. Solutions to mechanical structure imperfections included advanced micromachining processes, complicated mechanical structure designs, post-micromachining [5–7], etc. In a word, these imperfections were often minimized by expensive tooling processes.

Using control techniques to compensate for undesired dynamics caused by mechanical imperfections is promising for MEMS gyroscopes because they can be of low cost. However, it is a much more challenging task for the direct angle measurement than for the angular rate measurement. This is because, for the direct angle measurement, it needs to achieve both 'mode matching' and 'consistent vibration,' while not interfering with the precession of the proof mass. This research field is relatively new. Very few control algorithms were reported to achieve that, and they were all verified by numerical simulations, none by experimental results yet. Besides, in those approaches, researchers made various assumptions on the type of imperfections: some assumed no cross-axis damping forces and/or resilient forces, some assumed unknown but matched spring stiffness and/or damping coefficients along two principal axes, etc. But, one thing in common, they all assumed that the mass of the proof mass was known, even in the research of angular rate sensing.

Among those reports, Shkel *et al* assumed unknown but matched spring stiffness and zero cross-axis damping force for the imperfect gyroscope dynamics. They proposed using energy and angular momentum as the feedback terms to control the proof mass trajectory [8–10]. However, the effectiveness in the direct angle measurement was not explicitly shown. Piyabongkarn *et al* proposed an algorithm for the angle and angular rate sensing [11]. The effects from cross-axis damping forces and resilient forces were ignored, and the system stability was not theoretically proven. Park *et al* assumed zero cross-axis damping force [1]. They proposed an algorithm that consisted of energy controls and mode tuning controls to compensate those imperfections. The stability was theoretically proven. But their approach required a calibration phase prior to the normal operation. Note that implementing those three algorithms needs the measurements of both the proof mass position and the velocity.

This paper proposes a novel approach for the direct angle measurement when mechanical imperfections exist. Compared to existing approaches, the proposed method does not need to measure both the positions and velocities, and it works with few assumptions on uncertain system parameters. Most importantly, it does not need to know the mass of the

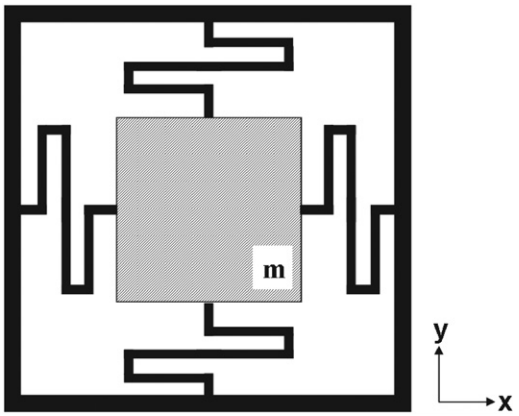

Figure 3. A design of a single-mass vibratory gyroscope.

proof mass beforehand, which is expected to further reduce the calibration work for MEMS vibratory gyroscopes. The proposed method was developed based on state estimation techniques. The system parameter estimation was skillfully arranged so that it can be done using various existing state observer algorithms and thus benefits from their advantages. The design procedures and stability analysis of the proposed method are discussed in detail.

2. Gyroscope dynamics

A MEMS gyroscope suitable for this application is shown in figure 3. It consists of a single proof mass suspended in a rigid frame by four flexures. Due to the symmetric design of the flexures, the proof mass can move freely in the xy plane. The dynamics of this gyroscope can be described as follows [3, 12–14]:

$$\begin{aligned} m\ddot{x} + d_{xx}\dot{x} + d_{xy}\dot{y} + k_{xx}x + k_{xy}y &= u_{sx} + 2m\Omega_z\dot{y}, \\ m\ddot{y} + d_{xy}\dot{x} + d_{yy}\dot{y} + k_{xy}x + k_{yy}y &= u_{sy} - 2m\Omega_z\dot{x}, \end{aligned} \tag{1}$$

where m is the mass of the proof mass; d_{xx}, d_{yy} and k_{xx}, k_{yy} are damping coefficients and spring stiffnesses along the two principal axes, respectively; Ω_z is the angular rate to be measured; d_{xy} and k_{xy} are respectively the cross-axis damping coefficient and spring stiffness; u_{sx} and u_{sy} are the control inputs along the x and y axes, respectively. Note that the angular acceleration terms ($m\dot{\Omega}_z y$, $m\dot{\Omega}_z x$) and centrifugal force terms $\left(m\Omega_z^2 x, m\Omega_z^2 y\right)$ have been omitted from (1). The angular acceleration terms were omitted by assuming that the measured angular rate is almost constant over a long enough time; the centrifugal force terms were omitted by designing the spring stiffness of the device much larger than the measured angular rates.

As discussed before, mechanical imperfections are inevitably present in MEMS devices. In this vibratory gyroscope design, imperfections mainly contribute to the existence of d_{xy} and k_{xy} and uncertain values of all system parameters including spring stiffness, damping coefficients and the mass. To have precise measurements of angular information from gyroscopes, these uncertain values must be either calibrated prior to practical use or their influence must be compensated in real time.

3. Feedback controls of gyroscope systems

This paper uses control methods to compensate for the dynamics alternation caused by mechanical imperfections. Assuming that unknown system parameters and the angular rate are constants, the dynamic equations of a vibratory gyroscope can be reformulated into the following:

$$\begin{aligned} \dot{X}_s &= f_s(X_s) + B_s U_s, \\ Z_s &= C_s X_s + N, \\ X_s &= \left[x \;\; y \;\; \dot{x} \;\; \dot{y} \;\; \Omega_z \;\; \tfrac{k_{xx}}{m} \;\; \tfrac{k_{yy}}{m} \;\; \tfrac{k_{xy}}{m} \;\; \tfrac{d_{xx}}{m} \;\; \tfrac{d_{yy}}{m} \;\; \tfrac{d_{xy}}{m} \;\; \tfrac{1}{m}\right]^T, \\ f_s(X_s) &= \begin{bmatrix} \dot{x} \\ \dot{y} \\ -\frac{k_{xx}}{m}x - \frac{k_{xy}}{m}y - \frac{d_{xx}}{m}\dot{x} - \frac{d_{xy}}{m}\dot{y} + 2\Omega_z\dot{y} \\ -\frac{k_{xy}}{m}x - \frac{k_{yy}}{m}y - \frac{d_{xy}}{m}\dot{x} - \frac{d_{yy}}{m}\dot{y} - 2\Omega_z\dot{x} \\ 0 \\ \vdots \\ 0 \end{bmatrix}_{12\times 1}, \\ B_s &= \begin{bmatrix} 0 & 0 & \frac{1}{m} & 0 \\ 0 & 0 & 0 & \frac{1}{m} \end{bmatrix}_{2\times 8}^T, \\ C_s &= \begin{bmatrix} 0 & 0 & 1 & 0 \\ 0 & 0 & 0 & 1 \end{bmatrix} [0]_{2\times 8}, \\ U_s &= [u_{sx} \quad u_{sy}]^T, \qquad N = [n_x \quad n_y]^T, \end{aligned} \tag{2}$$

where N is the measurement noise of the gyroscope system; X_s is a state vector consisting of system dynamics (proof mass position and velocity), unknown system parameters and the angular rate. C_s denotes the measurement of this gyroscope system. Normally, they were the proof mass positions and/or velocities. The proposed method only needs either one of them. Here, we demonstrate the control method using measurements of the proof mass velocity.

The assumption of constant system parameters and angular rate is impractical in real applications. When these unknown values are time varying, their effects are treated as modeling error and minimized by the robustness of the proposed control method.

3.1. State observer design

For system equations shown in (2), a state observer can be constructed to estimate the proof mass dynamics and system parameters simultaneously:

$$\begin{aligned} \dot{\hat{X}}_s &= f_s(\hat{X}_s) + B_s(\hat{m})U_s + L_s(Z_s - \hat{Z}_s), \\ \hat{Z}_s &= C_s\hat{X}_s, \end{aligned} \tag{3}$$

where $\hat{X}_s$ is the estimation of X_s; L_s is the observer gain matrix, which can be obtained from various existing observer algorithms. The observer gain matrix can be divided into L_{s1} and L_{s2} with proper dimensions. L_{s1} is the feedback gain for the estimation of the proof mass dynamics, while L_{s2} is for the system parameters.

Here, for the proof of system stability, we derive the observer gain using Lyapunov theory. L_{s1} and L_{s2} are chosen as follows to ensure the correct estimation of all states in X_s:

$$L_s^T = \left[L_{s1}^T L_{s2}^T\right],$$
$$L_{s1}^T = \begin{bmatrix} 0 & 0 & l_{s31} & 0 \\ 0 & 0 & 0 & l_{s42} \end{bmatrix}, \tag{4}$$
$$L_{s2}^T = \begin{bmatrix} 2\dot{\hat{y}} & -\hat{x} & 0 & -\hat{y} & -\dot{\hat{x}} & 0 & -\dot{\hat{y}} & u_{sx} \\ -2\dot{\hat{x}} & 0 & -\hat{y} & \hat{x} & 0 & -\dot{\hat{y}} & -\dot{\hat{x}} & u_{sy} \end{bmatrix},$$

where l_{s31} and l_{s42} can be any positive numbers.

As discussed before, the error due to time-varying system parameters and time-varying angular rates can be minimized by the robustness of the feedback controller design. In the proposed method, it is minimized by the robustness of the observer design. Besides the proposed method, other applicable observer algorithms include extended Kalman filter with fading memory [15], sliding observers [16], etc.

3.2. Feedback controller design

The observability of a system can be altered by the applied feedback controller. Thus, two main tasks for the feedback controller are as follows: (1) to meet the 'observability [17]' requirements so that all states in X_s can be correctly estimated, and (2) to regulate the proof mass trajectory so that the direct calculation of the rotation angle can be processed subsequently. To achieve these two goals, the control inputs are designed as follows:

$$U_s = \begin{bmatrix} u_{sx} \\ u_{sy} \end{bmatrix} = \hat{m} \begin{bmatrix} \frac{\hat{d_{xx}}}{\hat{m}}\dot{\hat{x}} + \frac{\hat{d_{xy}}}{\hat{m}}\dot{\hat{y}} + \frac{\hat{k_{xx}}}{\hat{m}}\hat{x} + \frac{\hat{k_{xy}}}{\hat{m}}\hat{y} - \omega_0^2\hat{x} + \beta_x \\ \frac{\hat{d_{xy}}}{\hat{m}}\dot{\hat{x}} + \frac{\hat{d_{yy}}}{\hat{m}}\dot{\hat{y}} + \frac{\hat{k_{xy}}}{\hat{m}}\hat{x} + \frac{\hat{k_{yy}}}{\hat{m}}\hat{y} - \omega_0^2\hat{y} + \beta_y \end{bmatrix}, \tag{5}$$

where ω_0 is the designated resonant frequency of the compensated system; β_x and β_y are two signals independent of state feedback. This independence requirement is mainly for estimating the quantity of the proof mass. Other requirements for selecting β_x and β_y will be discussed shortly.

Once the estimated outputs converge to the system measurements ($\hat{Z}_s \rightarrow Z_s$), the dynamics of the estimated states can be described as follows:

$$\begin{aligned} \ddot{\hat{x}} + \omega_0^2\hat{x} &= 2\hat{\Omega}_z\dot{\hat{y}} + \beta_x, \\ \ddot{\hat{y}} + \omega_0^2\hat{y} &= -2\hat{\Omega}_z\dot{\hat{x}} + \beta_y. \end{aligned} \tag{6}$$

Furthermore, once the estimated state values converge to the correct state values $\hat{X}_s \rightarrow X_s$, equation (6) describes the proof mass dynamics of a compensated gyroscope system.

3.3. Angle calculation

In a special case when $\hat{\Omega}_z = \beta_x = \beta_y = 0$, the analytical solution of (6) is

$$\begin{aligned} \hat{x} &= a\cos\theta\cos\phi - b\sin\theta\sin\phi, \\ \hat{y} &= a\cos\theta\sin\phi + b\sin\theta\cos\phi, \\ \dot{\hat{x}} &= \omega_0(-a\sin\theta\cos\phi - b\cos\theta\sin\phi), \\ \dot{\hat{y}} &= \omega_0(-a\sin\theta\sin\phi + b\cos\theta\cos\phi), \end{aligned} \tag{7}$$

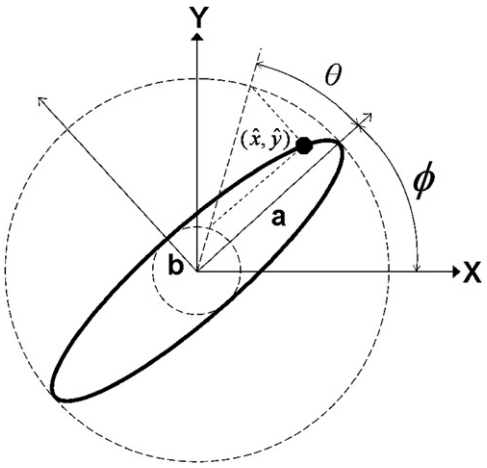

Figure 4. Ellipse trajectory of the proof mass when the gyroscope system is not rotating. The ellipse has a semi-major axis a, semi-minor axis b, an inclination angle ϕ and an orbital angle θ.

where $\theta = \omega_0 t + \theta_0$. The parameters a, b, ϕ and θ_0 are constants and depend on the initial conditions. This trajectory can be better visualized in figure 4. It is an ellipse with semi-major axis length a, semi-minor axis length b and an inclination angle ϕ from the X–Y coordinate.

Friedland and Hutton developed analytical solutions for the case when β_x and β_y in (6) are zero [2]. To work with our control method, we developed the analytical solution for (6) with the solution format completely imitating the one shown in (7). In that case, the parameters a, b, ϕ and θ become time varying and can be described as follows:

$$\begin{bmatrix} \dot{a} \\ \dot{b} \end{bmatrix} = \begin{bmatrix} -\hat{\Omega}_z b\sin 2\theta \\ \hat{\Omega}_z a\sin 2\theta \end{bmatrix} + \frac{1}{\omega_0}\begin{bmatrix} -\sin\theta & 0 \\ 0 & \cos\theta \end{bmatrix}\begin{bmatrix} \cos\phi & \sin\phi \\ -\sin\phi & \cos\phi \end{bmatrix}\begin{bmatrix} \beta_x \\ \beta_y \end{bmatrix},$$
$$\begin{bmatrix} \dot{\phi} \\ \dot{\theta} \end{bmatrix} = \begin{bmatrix} \frac{2\hat{\Omega}_z(b^2\cos^2\theta - a^2\sin^2\theta)}{a^2 - b^2} \\ \frac{-2\hat{\Omega}_z ab\cos 2\theta}{a^2 - b^2} + \omega_0 \end{bmatrix} + \frac{-1}{\omega_0(a^2 - b^2)} \times \begin{bmatrix} -b\cos\theta & a\sin\theta \\ a\cos\theta & -b\sin\theta \end{bmatrix}\begin{bmatrix} \cos\phi & \sin\phi \\ -\sin\phi & \cos\phi \end{bmatrix}\begin{bmatrix} \beta_x \\ \beta_y \end{bmatrix}, \tag{8}$$

where $\dot{\phi}$ in the above equation can be further processed and regrouped into three terms:

$$\begin{aligned} \dot{\phi} &= -\hat{\Omega}_z + F_{1H} + F_{2H}, \\ F_{1H} &= \frac{\hat{\Omega}_z\cos 2\theta(a^2 + b^2)}{a^2 - b^2}, \\ F_{2H} &= \frac{-1}{\omega_0(a^2 - b^2)}[-b\cos\theta \quad a\sin\theta] \times \begin{bmatrix} \cos\phi & \sin\phi \\ -\sin\phi & \cos\phi \end{bmatrix}\begin{bmatrix} \beta_x \\ \beta_y \end{bmatrix}. \end{aligned} \tag{9}$$

Most MEMS vibratory gyroscopes measure angular rates with a range around $\pm$ 300° s^{-1} and a bandwidth of a few hundred Hz [18]. Therefore, if ω_0 is designed to be much larger than the measured angular rate, according to (8), $\dot{\theta} \approx \omega_0$.

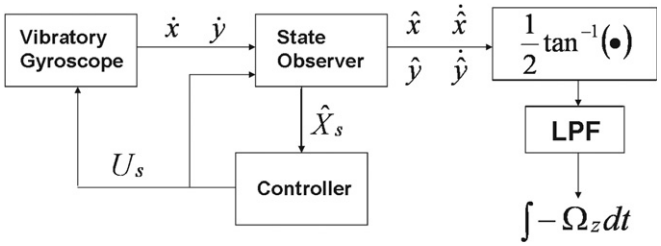

Figure 5. Signal process flow of the proposed direct angle measurement method.

Furthermore, $\hat{\Omega}_z$ is of a few hundred Hz and thus a low-frequency signal; F_{1H} is the $\hat{\Omega}_z$ modulated by the frequency $2\omega_0$; F_{2H} are the control inputs β_x and β_y modulated by both ω_0 and the frequency of $\hat{\Omega}_z$. Therefore, if the frequency contents of β_x and β_y are designed to be distant from ω_0 and the frequency content of Ω_z, $\hat{\Omega}_z$ in (9) can be separated from F_{1H} and F_{2H} using a low pass filter. This leads to the following:

$$\phi = \int \dot{\phi}\,\mathrm{d}t = \int -\hat{\Omega}_z\,\mathrm{d}t + \int F_{1H}(\cdot)\,\mathrm{d}t + \int F_{2H}(\cdot)\,\mathrm{d}t,$$
$$\int -\hat{\Omega}_z\,\mathrm{d}t = \mathrm{LPF}(\phi), \tag{10}$$

where LPF$(\cdot)$ stands for a filtered signal from a low pass filter. Note that the angle ϕ does not need to come from (9). It can be calculated from (11) according to the ellipse trajectory shown in figure 4:

$$\phi = \frac{1}{2}\tan^{-1}\frac{2\left(\omega_0^2\hat{x}\,\hat{y} + \dot{\hat{x}}\,\dot{\hat{y}}\right)}{\omega_0^2(\hat{x}^2 - \hat{y}^2) + (\dot{\hat{x}}^2 - \dot{\hat{y}}^2)}. \tag{11}$$

Thus, we can obtain the rotation angle from the instantaneous values of the estimated proof mass dynamics.

3.4. Signal process flow

The signal process steps of the proposed direct angle measurement are summarized as follows. From the measured proof mass velocities, the state observer calculated the estimated proof mass dynamics and system parameters. These estimated values were fed back to regulate the proof mass trajectory and to calculate ϕ using (11). This calculated angle value is then sent to a low pass filter. The output of the low pass filter is equivalent to the integration of the estimated angular rate. If the estimated angular rate converges to the angular rate to be measured due to the proposed feedback controller design, this algorithm obtains the rotation angle without integrating angular rates. The signal processing flow is shown in figure 5.

4. Stability analysis

The proposed feedback controller design is essentially a task of stabilizing a nonlinear system using estimated system dynamics and parameters. For the stability analysis, we first show the observability of the system, and then the state convergence of the proposed feedback controller design.

4.1. System observability

The success of state estimations depends on the observability of a system, which can be examined by the rank of the corresponding observability matrix. The observability matrix of a nonlinear system can be obtained as follows [17]:

$$W_{so} \equiv \frac{\partial}{\partial X_s}[Z_s \quad \dot{Z}_s \quad \ddot{Z}_s \quad \cdots]. \tag{12}$$

For this feedback control gyroscope system, we examine up to the fourth derivative of the system outputs. In that case, the observability matrix (W_{so}) has the following format:

$$W_{so} = \begin{bmatrix} [W_{ss}]_{4\times4} & [0]_{4\times8} \\ [0]_{8\times4} & [W_{sp}]_{8\times8} \end{bmatrix}_{12\times12}. \tag{13}$$

After tedious derivations, the above W_{ss} and W_{sp} matrices can be greatly simplified as follows:

$$W_{ss} = \begin{bmatrix} 0 & 0 & 1 & 0 \\ 0 & 0 & 0 & 1 \\ -\frac{k_{xx}}{m} & -\frac{k_{xy}}{m} & 0 & 0 \\ -\frac{k_{xy}}{m} & -\frac{k_{yy}}{m} & 0 & 0 \end{bmatrix},$$

$$W_{sp} = \begin{bmatrix} 2\ddot{y} & -\dot{x} & 0 & -\dot{y} & -\ddot{x} & 0 & -\ddot{y} & \dot{u}_{sx} \\ -2\ddot{x} & 0 & -\dot{y} & -\dot{x} & 0 & -\ddot{y} & -\ddot{x} & \dot{u}_{sy} \\ 2y^{(3)} & -\ddot{x} & 0 & -\ddot{y} & -x^{(3)} & 0 & -y^{(3)} & \ddot{u}_{sx} \\ -2x^{(3)} & 0 & -\ddot{y} & -\ddot{x} & 0 & -y^{(3)} & -x^{(3)} & \ddot{u}_{sy} \\ 2y^{(4)} & -x^{(3)} & 0 & -y^{(3)} & -x^{(4)} & 0 & -y^{(4)} & u_{sx}^{(3)} \\ -2x^{(4)} & 0 & -y^{(3)} & -x^{(3)} & 0 & -y^{(4)} & -x^{(4)} & u_{sy}^{(3)} \\ 2y^{(5)} & -x^{(4)} & 0 & -y^{(4)} & -x^{(5)} & 0 & -y^{(5)} & u_{sx}^{(4)} \\ -2x^{(5)} & 0 & -y^{(4)} & -x^{(4)} & 0 & -y^{(5)} & -x^{(5)} & u_{sy}^{(4)} \end{bmatrix}. \tag{14}$$

Due to a diagonal form of W_{so}, W_{ss} is the observability matrix of the proof mass dynamics (x, y, $\dot{x}$, $\dot{y}$) and W_{sp} is the observability matrix for the unknown system parameters.

According to (14), the rank of W_{ss} is 4 when $k_{xx}k_{yy} \neq k_{xy}^2$. In that case, those four states are globally observable. Similarly, the rank of W_{sp} needs to be 8 for the correct estimation of all unknown system parameters. As shown in W_{sp}, its rank depends on the proof mass trajectory and thus influenced by the feedback controller design. It can be shown that the rank of W_{sp} is 8 when two conditions are met: (1) the proof mass trajectory contains more than one frequency; (2) β_x and β_y are bounded signals and $\dot{\beta}_x$ and $\dot{\beta}_y$ are nonzero.

4.2. Stability analysis

The stability of this control system is proven by the Lyapunov stability theorem [17]. The error dynamics ($\underline{e} \triangleq X_s - \hat{X}_s$) can be obtained by subtracting (2) from (3), which leads to the following:

$$\dot{\underline{e}} = -(L_s C_s + \widetilde{F})\underline{e},$$
$$\underline{e}^T = \begin{bmatrix} \tilde{e_1}^T & \tilde{e_2}^T & \tilde{\theta}^T \end{bmatrix},$$
$$\tilde{e_1}^T = [e_x \quad e_y],$$

$$\tilde{e_2}^T = [e_{\dot{x}} \quad e_{\dot{y}}],$$

$$\tilde{\theta}^T = \left[e_{\Omega_z} \quad e_{\frac{k_{xx}}{m}} \quad e_{\frac{k_{yy}}{m}} \quad e_{\frac{k_{xy}}{m}} \quad e_{\frac{d_{xx}}{m}} \quad e_{\frac{d_{yy}}{m}} \quad e_{\frac{d_{xy}}{m}} \quad e_{\frac{1}{m}}\right],$$

$$\tilde{F}^T = \begin{bmatrix} 0 & 0 & \frac{k_{xx}}{m} & \frac{k_{xy}}{m} \\ 0 & 0 & \frac{k_{xy}}{m} & \frac{k_{yy}}{m} \\ -1 & 0 & \frac{d_{xx}}{m} & \left(\frac{d_{xy}}{m} + 2\Omega_z\right) \\ 0 & -1 & \left(\frac{d_{xy}}{m} - 2\Omega_z\right) & \frac{d_{yy}}{m} \\ 0 & 0 & -2\dot{\hat{y}} & 2\dot{\hat{x}} \\ 0 & 0 & \hat{x} & 0 \\ 0 & 0 & 0 & \hat{y} \\ 0 & 0 & \hat{y} & \hat{x} \\ 0 & 0 & \dot{\hat{x}} & 0 \\ 0 & 0 & 0 & \dot{\hat{y}} \\ 0 & 0 & \dot{\hat{y}} & \dot{\hat{x}} \\ 0 & 0 & -u_{sx} & -u_{sy} \end{bmatrix} [0]_{12\times 8}. \tag{15}$$

A Lyapunov function is chosen as

$$V = \frac{1}{2}\underline{e}^T P \underline{e},$$

$$P = \begin{bmatrix} \begin{bmatrix} \frac{k_{xx}}{m} & \frac{k_{xy}}{m} & 0 & \frac{d_{xy}}{m} \\ \frac{k_{xy}}{m} & \frac{k_{yy}}{m} & \frac{d_{xy}}{m} & 0 \\ 0 & 0 & 1 & 0 \\ 0 & 0 & 0 & 1 \end{bmatrix} & [0]_{4\times 8} \\ [0]_{8\times 4} & [I]_{8\times 8} \end{bmatrix}. \tag{16}$$

The above P matrix is positive definite if $k_{xx}k_{yy} > k_{xy}^2$. Using the observer gain L_s shown in (4), the derivative of the Lyapunov function is greatly simplified to the following:

$$\dot{V} = -\tilde{e_2}^T \begin{bmatrix} \frac{d_{xx}}{m} + l_{s31} & 0 \\ 0 & \frac{d_{yy}}{m} + l_{s42} \end{bmatrix} \tilde{e_2}. \tag{17}$$

The above equation is negative semi-definite, which implies that the system is stable and all states in $\underline{e}$ are bounded. Furthermore, according to (15), the value of $\dot{\underline{e}}$ is also bounded.

Taking one more derivative of (17) leads to the following:

$$\ddot{V} = -2\dot{\underline{e}}^T (LC + \tilde{F})^T P \underline{e} - \underline{e}^T (\dot{L}C + \dot{\tilde{F}})^T P \underline{e}. \tag{18}$$

$\ddot{V}$ is bounded because each term on the right-hand side of (18) is bounded. According to Barbalat's lemma [17], $\dot{V}$ converges to zero as time approaches infinity. Thus,

$$\|\tilde{e_2}\| \to 0. \tag{19}$$

After each state in $\tilde{e_2}$ converging to zero, equation (15) can be simplified and rearranged as follows:

$$\Lambda \dot{\tilde{e}}_1 = -W^T(\hat{x},\ \dot{\hat{x}},\ \hat{y},\ \dot{\hat{y}})\tilde{\theta},$$

$$\Lambda = \begin{bmatrix} \frac{k_{xx}}{m} & \frac{k_{xy}}{m} \\ \frac{k_{xy}}{m} & \frac{k_{yy}}{m} \end{bmatrix},$$

$$W^T = \begin{bmatrix} -2\dot{\hat{y}} & \hat{x} & 0 & \hat{y} & \dot{\hat{x}} & 0 & \dot{\hat{y}} & -u_{sx} \\ 2\dot{\hat{x}} & 0 & \hat{y} & \hat{x} & 0 & \dot{\hat{y}} & \dot{\hat{x}} & -u_{sy} \end{bmatrix}. \tag{20}$$

Since each term in the above equation is bounded, taking the integration of the above equation leads to the following:

$$\int_0^\infty \Lambda \tilde{e}_1 \mathrm{d}t = -\int_0^\infty W^T \tilde{\theta}\ \mathrm{d}t = -\bar{W}^T\tilde{\theta}\big|_0^\infty + \int_0^\infty \bar{W}^T\dot{\tilde{\theta}}\ \mathrm{d}t,$$

$$\bar{W}^T = \int W^T\ \mathrm{d}t. \tag{21}$$

W consists of estimated proof mass dynamics only, once $\tilde{e_2}$ is zero, whose values are governed by (6). Therefore, $\bar{W}$ is bounded. Using the triangle inequality, one can obtain the following:

$$\left\| \int_0^\infty \Lambda \tilde{e}_1\ \mathrm{d}t \right\| \leqslant \|\bar{W}^T\tilde{\theta}|_0^\infty\| + \|\bar{W}^T\|_\infty \cdot \|\tilde{\theta}|_0^\infty\|. \tag{22}$$

Again, since each term on the right-hand side of the above equation is bounded, from (20) and (22), the following two conditions are met:

$$\lim_{t\to\infty} \|\tilde{e_1}\| \to 0,$$
$$\lim_{t\to\infty} W^T\tilde{\theta} \to 0. \tag{23}$$

According to the equation above, $\tilde{\theta}$ would converge to zero only if the row rank of W is 8. This can be verified by examining the rank of the following matrix:

$$[W \quad \dot{W} \quad \ddot{W} \cdots]. \tag{24}$$

Note that the above matrix is almost the same as the observability matrix of the system parameters W_{sp}; only the real state trajectory is replaced by the estimated state trajectory described in (6). Therefore, as long as the frequency content of β_x and β_y is not ω_0, the estimated trajectory contains more than one frequency, and thus $\tilde{\theta}$ converges to zero.

Combining the above conclusions, (19) and (23), one can show that $\underline{e} \to 0$. Therefore, the estimated system dynamics and parameters converge to their correct values, meaning that, in the steady state, the proof mass dynamics are the same as the estimated proof mass dynamics described in (6).

5. Simulations

In the numerical verification, the spring stiffness, damping coefficients, and the mass of a fabricated vibratory gyroscope are listed in table 1. These numbers are roughly the same as those of a fabricated MEMS gyroscope [19]. The measurements of the gyroscope system are the proof mass velocities along two axes, and are contaminated by zero-mean white noise with a standard deviation of 20 μm s^{-1}, which

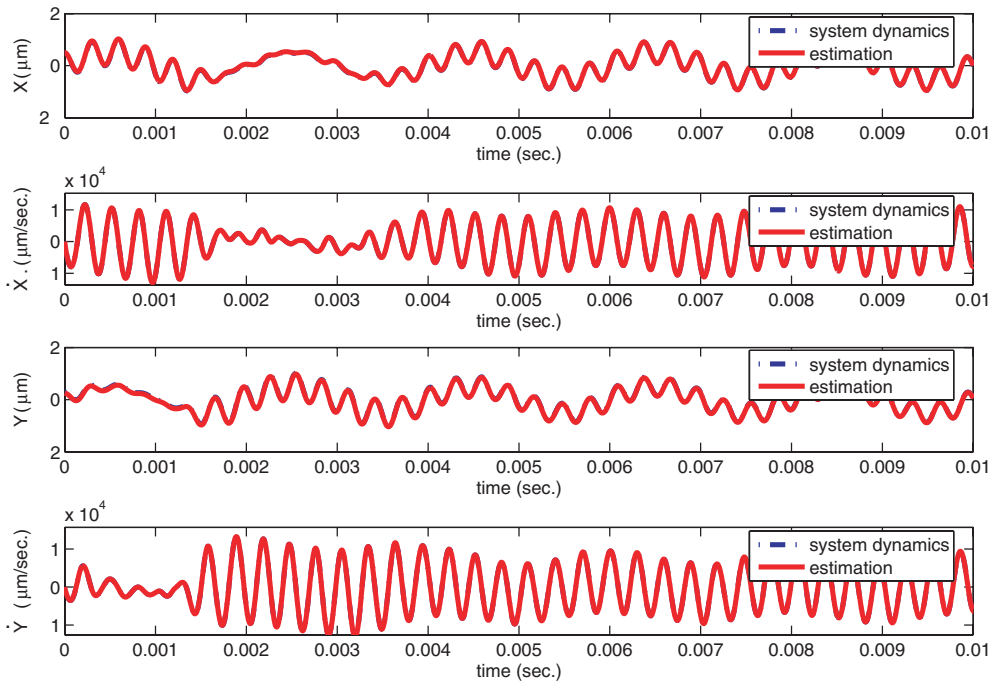

Figure 6. Estimation of the proof mass positions and velocities. The estimated values and correct values are almost identical.

Table 1. System parameters of a MEMS vibratory gyroscope.

Parameters	Values
m	1.8×10^{-7} kg
Ω_z	$0^\circ\ \mathrm{s}^{-1}$, $t \leqslant 0.5$ s
	$200 \sin(2\pi \times 10t)\ \mathrm{deg\,s}^{-1}$, $t \geqslant 0.5$ s
k_{xx}	$63.96\ \mathrm{N\,m}^{-1}$
k_{yy}	$95.92\ \mathrm{N\,m}^{-1}$
k_{xy}	$12.78\ \mathrm{N\,m}^{-1}$
d_{xx}	$3.6 \times 10^{-6}\ \mathrm{N\,s\,m}^{-1}$
d_{yy}	$4.5 \times 10^{-6}\ \mathrm{N\,s\,m}^{-1}$
d_{xy}	$3.6 \times 10^{-7}\ \mathrm{N\,s\,m}^{-1}$

equals a noise level of 0.1% FSO (full scale output). Note that MEMS gyroscopes having this measurement accuracy can normally achieve an accuracy of $1^\circ\ \mathrm{s}^{-1}$ for the angular rate sensing, on the premises that most system parameters are well calibrated [18].

In the feedback controller design, the designated resonant frequency ω_0 was designed to be $(2\pi \times 3.2 \times 10^3)$. Two control input signals were designed to be $\beta_x = \beta_y = 7.27 \times 10^{-6} \sin(2\pi \times 500t)N$. Ω_z was $200^\circ\ \mathrm{s}^{-1}$ with a frequency of 10 Hz. The sampling rate of the control algorithm was 200 kHz.

Figures 6 and 7 show the estimations of the proof mass dynamics and unknown system parameters. The initial guesses of those values were 20% off from their correct values. According to the plot, the estimated proof mass dynamics quickly converge to their correct values; the lines for the system dynamics and estimated ones overlap each other and thus are not clearly shown. Besides, the compensated dynamics show more than one frequency, which complies with the requirements of system observability. Calculating from 0.005 to 0.01 s, the standard deviations of the estimation errors are 0.01 μm, 3.45 $\mu\mathrm{m\,s}^{-1}$, 0.02 μm and 4.26 $\mu\mathrm{m\,s}^{-1}$ for x, $\dot{x}$, y and $\dot{y}$, respectively.

The estimated system parameters converge to their correct values within 0.2 s. However, due to large noises present in the measured signals, the estimation oscillated a lot especially for the angular rate and damping terms. Calculating from 0.7 to 1 s, the estimation errors for the system parameters are as follows: the standard deviation of Ω_z is $226.3^\circ\ \mathrm{s}^{-1}$; the relative errors for the unknown system parameters m, k_{xx}, k_{yy}, k_{xy}, d_{xx}, d_{yy} and d_{xy} are 7.0×10^{-5}, 1.9×10^{-4}, 1.6×10^{-4}, 8.5×10^{-4}, 0.11, 0.06 and 1.36, respectively.

Figure 8 shows the compensated proof mass trajectory from 0.7 to 0.75 s, which is half of a rotation cycle. The precession of the proof mass is significantly interfered by the control inputs β_x and β_y. Thus, the suggested signal processing steps are required to facilitate the direct angle measurement.

The upper plot of figure 9 shows the frequency content of the estimated angle before low pass filtering. This frequency content can be grouped into three sets: the frequencies below 200 Hz, two resonance peaks at 2.7 and 3.7 kHz, and several resonance around 6.4 kHz. According to the analysis shown in (10), these three sets correspond to the frequency content of Ω_z, F_{2H} and F_{1H}, respectively. Therefore, using a low pass filter with the corner frequency of 200 Hz, the angular information is separated from the rest of signals, which is shown at the lower plot of figure 9. The low pass filter in this simulation was a fifth-order, digital, Butterworth filter.

Figure 10 shows angle estimations using the proposed method. Note that the low pass filtering introduces an 8°phase lag in the angle output. To better understand the error introduced by other means, the estimated angle was shifted $8^\circ$and compared to the angle to be measured. The simulation results showed that the standard deviation of the estimation

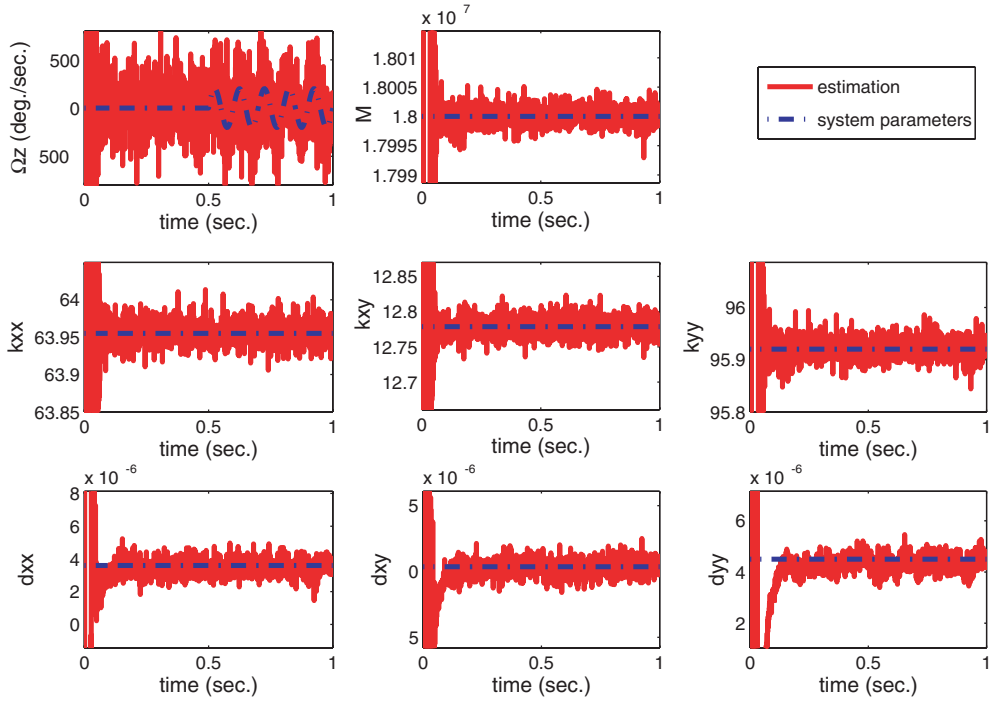

Figure 7. Estimation of eight unknown system parameters. The estimated values converge to their correct values within 0.2 s. The estimation of mass and spring stiffness is accurate, while the estimation of angular rates and damping coefficients is noisy.

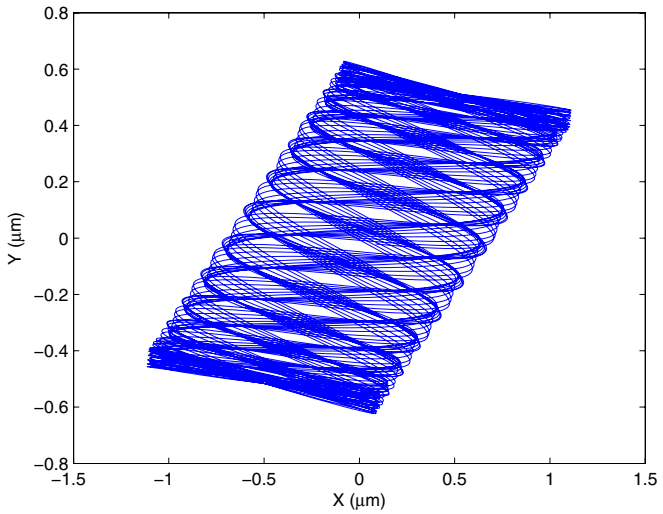

Figure 8. The compensated proof mass trajectory.

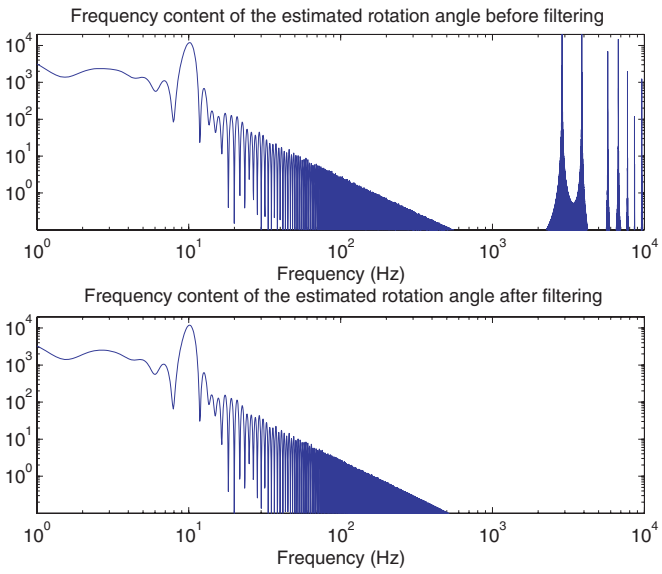

Figure 9. Frequency content of the estimated rotation angle before and after low pass filtering ($\simeq$ 200 Hz).

error was 0.23°. For comparison purposes, the angle obtained by integrating the angular rate is shown in the right column. The error drifts with time and the largest error is 1.5° within 1 s.

Figures 11 and 12 show the case when the system parameters are changed during operation, for example, damping increases at 0.5 s due to a leakage of the device package. The proposed method was able to compensate this sudden change and retained the rotation angles. Note that there exists a bias value in the estimated angle after 0.5 s. That is because the system loses track of rotation angles during the transient response of the parameter estimation and compensation.

6. Discussion

The proposed method is proven to be globally asymptotically stable in this problem definition (shown in section 4), meaning that the state/parameter convergence does not depend on the initial conditions. However, due to the presence of measurement noise and numerical computation errors, our simulation results showed that the state convergence occurred only when the initial estimation error is within $\pm$ 25%. In real applications, it may not be practical to estimate all the system

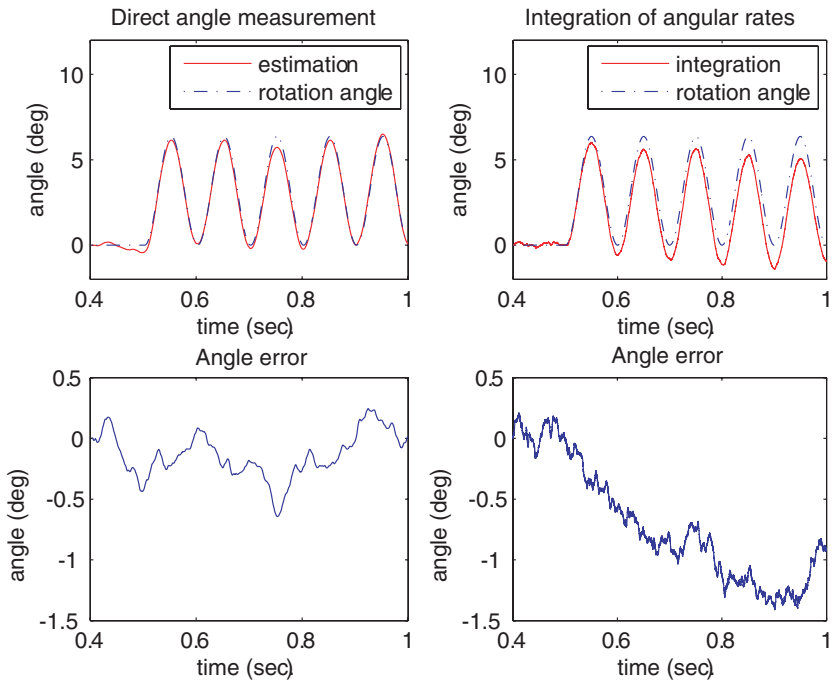

Figure 10. Angle estimations using the direct angle measurement method and integrating the angular rates.

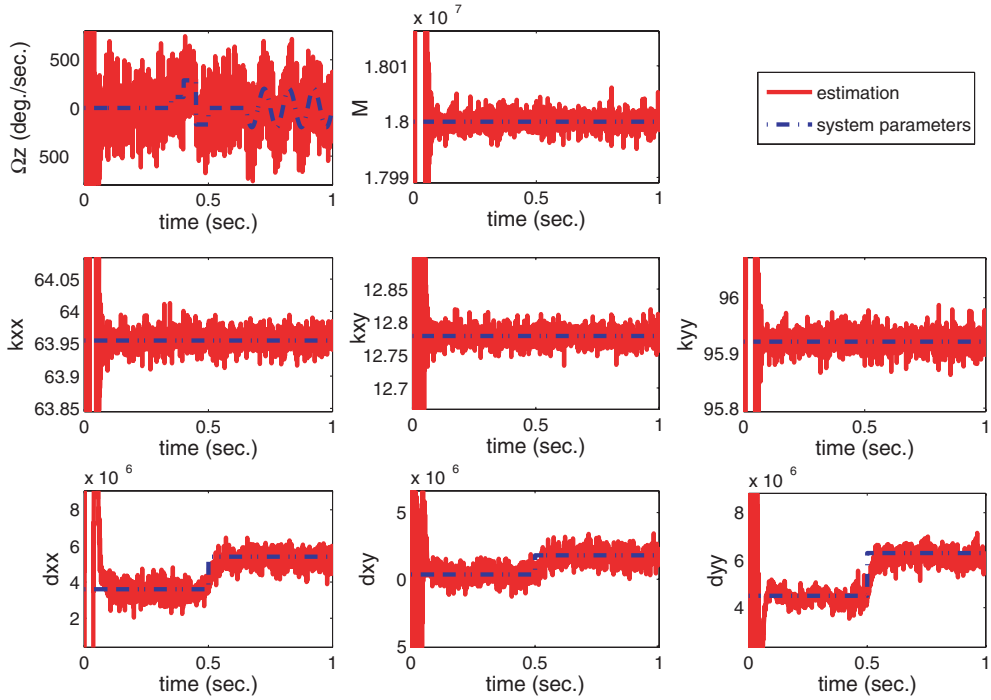

Figure 11. Estimations of eight unknown system parameters when the damping coefficients suddenly change at 0.5 s. The estimated values converge to their correct values.

parameters simultaneously and limit the frequency content of the proof mass trajectory to its minimum requirement. Our simulation results also showed that several properties can be improved when more frequencies are present in the proof mass trajectory and/or a smaller number of unknown parameters are estimated. These properties include convergence range, convergence speed, estimation accuracy and feedback control sampling rate.

One of the major concerns in MEMS vibratory gyroscopes is the temperature effect. The temperature variation may result in stress mismatch in packaging [20], variation of energy dissipation [21], variation of elastic modulus and film oxidation [22], which cause serious performance degradation for MEMS devices. Therefore, most quality MEMS gyroscopes integrate a temperature sensor into the device for temperature compensation. These temperature effects can be

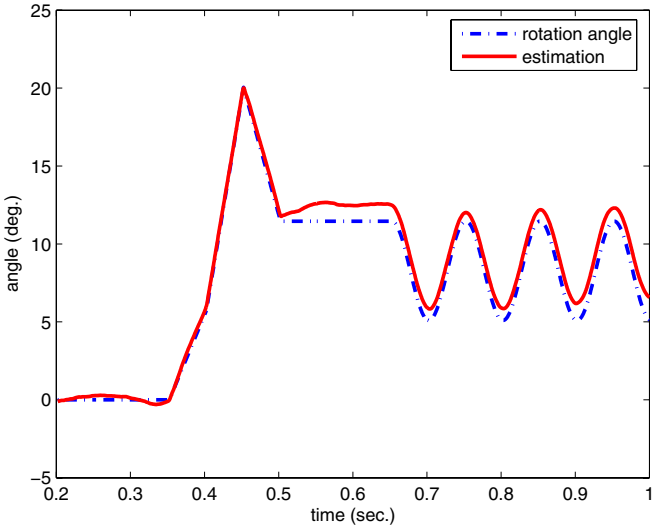

Figure 12. Angle determination using the proposed methods when the damping coefficients suddenly change at 0.5 s.

accounted as slow drifting system parameters, including the damping coefficient and spring stiffness [23]. Figure 11 shows that the proposed algorithm can track system parameters even when those parameters are changing with time. Therefore, we expect that, without using a temperature sensor, the proposed algorithm can compensate temperature effects for MEMS gyroscopes.

According to the simulation results shown in figure 10, the angle estimation error is 0.23°. This error may result from two paths: errors in the estimated states, which leads to angle errors when using (11); errors in the estimated system parameters, which leads to angle errors because the compensated gyroscope dynamics deviated from (6). Both these errors originate from the noise in the measured velocity signals. To clarify the influence of each path, we added the same amount of position/velocity errors as those shown in figure 6 to an 'ideal' gyroscope dynamics described by (6). The estimated angle accuracy was 0.037°. Therefore, we concluded that the angle accuracy of the proposed method is dominated by estimation errors of system parameters, particularly in the damping terms and angular rates.

The proposed signal processing can be done differently. An alternative approach is to use a bandpass filter, with the passband centered at ω_0 and the bandwidth twice that of the measured angles. According to the signal process flow shown in figure 13, this approach filters out the influence of β_x and β_y prior to the calculation of rotation angles. This approach is doable, but it requires a bandpass filter with a bandwidth twice that of the proposed approach. The major disadvantage is the noisy signal due to a large bandwidth.

Like most existing gyroscope control papers, this paper only discussed imperfections that can be attributed to uncertain system parameters. However, more imperfections exist in real applications such as unstructure dynamics, structure uncertainties, and angular accelerations. Although the proposed method can tolerate more parameter uncertainty than other control algorithms, it is possible that some imperfections that can be neglected in other control algorithms are crucial

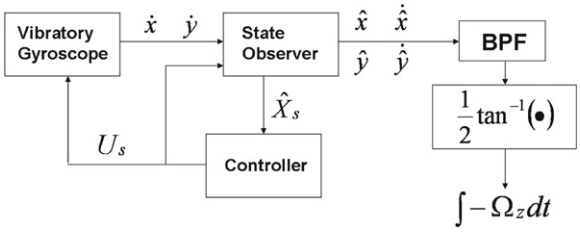

Figure 13. An alternative signal process flow using a bandpass filter.

to the proposed one. Therefore, other types of imperfection should be investigated and/or experiments using real devices should be performed to verify the feasibility of this method. When implementing the proposed algorithm in digital format, the major concern is the sampling rate 200 kHz. Since the proposed algorithm does not involve mass computations, the throughput of the digital controller is likely limited by the speed of the digital-to-analog converter (DAC). Currently, a 10 bit, 500 kHz DAC is classified as a middle-level product.

7. Conclusion

This paper proposed an online compensation method for a vibratory gyroscope for direct angle measurement. Using measured proof mass velocities only, the proposed method can oscillate the proof mass along two axes at a designated frequency while preserving its precession motion, when mechanical imperfections exist. The rotation angle was directly calculated without integrating angular rates.

The proposed method can compensate for imperfections including unknown proof mass, unknown cross-axis spring stiffness and damping coefficients, unknown and unmatched spring stiffness and damping coefficients along the two principal axes. Our analysis showed that when all these imperfections exist simultaneously, the proposed method can compensate for their influences on two conditions: the regulated proof mass trajectory contains more than one frequency, control inputs contain signals that are independent of state feedback and the first derivatives of those signals are nonzero.

Simulation results showed that the proposed method can compensate for imperfections even when those system parameters change with time. In a simulation case, the imperfections caused all the system parameters to be 20% off from their designated values; the measured signals were the proof mass velocities along the two principal axes and the noise level was 0.1% FSO; the proposed method can obtain correct rotation angle with an angle accuracy of 0.23°. This angle measurement accuracy is dominated by the error in estimating system parameters, which originated from the noise in the measured velocity signals.

References

[1] Park S, Horowitz R and Tan C W 2008 Dynamics and control of a MEMS angle measuring gyroscope *Sensors Actuators* A **144** 56–63

[2] Friedland B and Hutton M 1978 Theory and error analysis of vibrating-member gyroscope *IEEE Trans. Autom. Control* **23** 545–56
[3] Shkel A, Howe R T and Horowitz R 1999 Modeling and simulation of micromachined gyroscopes in the presence of imperfections *Int. Conf. on Modelling and Simulation of Microsystems (Puerto Rico)* pp 605–8
[4] Weinberg M S and Kourepenis A 2006 Error sources in in-plane silicon tuning-fork MEMS gyroscopes *J. Microelectromech. Syst.* **15** 479–91
[5] Kawai H, Atsuchi K I, Tamura M and Ohwada K 2001 High-resolution microgyroscope using vibratory motion adjustment technology *Sensors Actuators* A **90** 153–9
[6] Alper S E and Akin T 2002 A symmetric surface micromachined gyroscope with decoupled oscillation modes *Sensors Actuators* A **97–98** 347–58
[7] Gunthner S, Egretzberger M, Kugi A, Kapser K, Hartmann B, Schmid U and Seidel H 2006 Compensation of parasitic effects for a silicon tuning fork gyroscope *IEEE Sensors* **6** 596–604
[8] Shkel A M, Horowitz R, Seshia A A, Park S and Howe R T 1999 Dynamics and control of micromachined gyroscopes *Proc. American Control Conf.* pp 2119–24
[9] Painter C and Shkel A 2003 Detection of orientation and predicted performance of a MEMS absolute angle measuring gyroscope *Proc. 4th Int. Workshop on Structural Health Monitoring* pp 1011–8
[10] Painter C and Shkel A 2005 Experimental evaluation of a control system for an absolute angle measuring micromachined gyroscope *IEEE Sensors* pp 1084–7
[11] Piyabongkarn D, Rajamani R and Greminger M 2005 The development of a MEMS gyroscope for absolute angle measurement *IEEE Trans. Control Syst. Technol.* **13** 185–95
[12] Park S and Horowitz R 2001 Adaptive control for *z*-axis MEMS gyroscopes *Proc. American Control Conf.* pp 1223–8
[13] Leland R P 2006 Adaptive control of a MEMS gyroscope using Lyapunov methods *IEEE Trans. Control Syst. Technol.* **14** 278–83
[14] Dong L, Zheng Q and Gao Z 2008 On control system design for the conventional mode of operation of vibrational gyroscopes *IEEE Sensors* **8** 1871–8
[15] Chi C Y and Chen T L 2009 Compensation of imperfections for vibratory gyroscope systems using state observers *Sensors Transducers J.* **6** 128–45
[16] Spurgeon S K 2008 Sliding mode observers Ga survey *Int. J. Syst. Sci.* **39** 751–64
[17] Vidyasagar M 1993 *Nonlinear Systems Analysis* (Englewood Cliffs, NJ: Prentice-Hall)
[18] Alper S E and Akin T 2005 A single-crystal silicon symmetrical and decoupled MEMS gyroscope on an insulating substrate *J. Microelectromech. Syst.* **14** 707–17
[19] Clark W A 1997 Micromachined vibratory rate gyroscopes *PhD Dissertation* University of California, Berkeley, CA
[20] Joo J W and Choa S H 2007 Deformation behavior of MEMS gyroscope sensor package subjected to temperature change *IEEE Trans. Compon. Packag. Technol.* **30** 346–54
[21] Kim B *et al* 2008 Temperature dependence of quality factor in MEMS resonators *J. Microelectromech. Syst.* **17** 755–66
[22] Jeong J H, Chung S H, Lee S H and Kwon D 2003 Evaluation of elastic properties and temperature effects in Si thin films using an electrostatic microresonator *J. Microelectromech. Syst.* **12** 524–30
[23] Shcheglov K, Evans C, Gutierrez R and Tang T K 2000 Temperature dependent characteristics of the JPL silicon MEMS gyroscope *IEEE Aerospace Conf. Proc.* **1** 403–11